# Time-dependent theory of multiphoton ionization of xenon

K. C. Kulander
*Theoretical Atomic and Molecular Physics Group, Lawrence Livermore National Laboratory, P.O. Box 808, Livermore, California 94550*
(Received 25 January 1988)

Calculations of the single and multiphoton ionization of xenon valence-shell electrons are reported for several wavelengths and laser intensities. The model follows a single valence electron in the field of an effective core potential, the remaining valence electrons, frozen in their ground-state orbitals, and a linearly polarized laser field. Ionization rates and cross sections are determined using a direct numerical solution of the time-dependent Schrödinger equation using a finite-difference technique. Excellent agreement with experimental rates and previous theoretical cross sections has been obtained. Bound states, shifted into resonance by the ac Stark effect, are found to affect the ionization dynamics. Departures from perturbation theory at high intensities are demonstrated and discussed.

## I. INTRODUCTION

Multiphoton ionization of atoms by intense laser fields has been the subject of active theoretical and experimental interest in recent years. Short pulsed lasers are capable of delivering peak powers which produce rapid, multiple ionization of isolated atoms in a single pulse. Theoretical treatments of these processes require a nonperturbative approach because the strengths of the electromagnetic fields due to the laser can exceed the Coulomb interactions in the atom. Also, the excitation, ionization processes take place on a time scale such that the temporal pulse shape can play a significant role in the product states produced. In many instances, the atom will be predicted to be ionized before the laser pulse has reached its maximum intensity.[1]

To study these phenomena, several groups[2–6] have found it convenient to employ a time-dependent picture to investigate the preionization dynamics of the atom, i.e., to understand how the laser energy is deposited in the atom, to determine whether collective excitation of several electrons can play a significant role in producing the observed rapid ionization, and to determine the energy spectrum of the emitted electrons. To date, calculations have been performed mostly on model systems or on atoms with only one or, at most, two electrons. We have developed a time-dependent Hartree-Fock (TDHF) model,[7] which is capable of representing truly multielectron atoms under the influence of a strong, pulsed laser field of arbitrary pulse shape, wavelength, and peak intensity. Our TDHF calculations on helium have produced a considerable amount of information about its ionization behavior.[8] This paper reports an initial step toward extending the TDHF technique to systems with more electrons.

We have performed calculations of the multiphoton ionization of electrons from the outer shell of xenon. The model of xenon we have employed is a frozen, single-electron picture, similar to one we used in helium, based on the Hartree-Fock wave function. We have constructed an effective potential for the core electrons using a Hartree-Slater (local) approximation for the exchange terms. From this, we calculate the ground-state orbitals for the outer $5s$ and $5p$ electrons, then freeze all but one of these electrons. The free electron is allowed to interact with the laser field, and its ionization probability (rate) is determined by explicitly solving the time-dependent Schrödinger equation for its wave function. The final state is determined by projecting the time-dependent wave function onto field-free states. We have examined the excitation and ionization dynamics for a number of wavelengths and intensities. This single-electron model was found to be very useful in our previous studies on helium.

A long history of theoretical treatments of multiphoton ionization of atoms using perturbation theory techniques has been able to explain most of the experimental observations.[9] Only recently have pulse lengths and peak intensities become large enough that the development of new theoretical methods has become necessary. The results reported here help to illustrate the multiphoton excitation and ionization process without the complications of many electrons, but for a realistic, three-dimensional system. They will assist in the interpretation of the multielectron calculations which will follow.

In Sec. II, the method used in these calculations is described. Section III contains the results of our calculations, and comparisons to previous theoretical and experimental work. Some conclusions about multiphoton ionization in this system, and directions for future work, including the extension of these calculations to the case where all the valence electrons are free to interact among themselves and with the laser field, are discussed in Sec. IV.

## II. METHOD

The frozen, single-electron model used in these calculations is an approximation to the TDHF picture. Here by

 

frozen we are referring to the orbitals of all but one of the electrons which remain fixed throughout the calculation. We begin with the time-dependent Schrödinger equation for an atom, initially in its field-free ground electronic state, subjected to a time-varying laser pulse giving

$$i\frac{\partial}{\partial t}\Psi(r,t)=(H_0+V_I)\Psi(r,t)\ , \tag{1}$$

where $H_0$ is the atomic Hamiltonian. The interaction term, given by

$$V_I=-\sum_i eE(t)z_i\sin(\omega t)\ , \tag{2}$$

assumes that the laser field, linearly polarized in the $z$ direction, can be treated classically and that the dipole approximation is valid. Both these assumptions are very accurate for the intensities and wavelengths we have considered. We approximate the electronic wave function by an antisymmetrized product of single-particle orbitals. Putting this determinental wave function into Eq. (1) gives the TDHF equations derived and discussed before.[8] This is a set of coupled partial differential equations for the time-dependent orbitals.

The TDHF equations are, in fact, too complex for numerical solution due to the presence of nonlocal exchange terms. Because we need to solve these equations thousands of times for a single calculation, we employ the local free-electron-gas exchange potential of Slater,

$$V_{\rm XC}(\mathbf{r})=\alpha[3\rho(\mathbf{r})/8\pi]^{1/3}\ , \tag{3}$$

with the modification, described by Herman and Skillman,[10] which assures the long-range behavior of the total potential is $-1/r$. The strength $\alpha$ of the exchange term was varied until the correct ionization energy, 12.13 eV, was obtained using a standard Hartree-Slater code. We ignore spin-orbit terms in the Hamiltonian and therefore the existence of the second ionization threshold at 13.4 eV corresponding to the $^2P_{1/2}$ state of the ion. Thus we calculate ionization into a single continuum only. We do not expect this to affect the rates appreciably for nonresonant wavelengths, but miss the transitions to the Rydberg series which converge to this second limit if they are important at these intensities.

The orbitals in the valence shell ($5s$ and $5p$) thus obtained were used to construct an effective core potential[11] after making them nodeless, as prescribed by Christiansen.[12] A single effective core potential, independent of angular momentum, is used in our calculations. The reason for this is that the final state in a many-photon ionization process will have many orbital angular momentum components, and it is not feasible to perform an angular momentum decomposition for the multielectron cases we wish to treat eventually. Since we are working toward this goal, it makes practical sense to perform the single-electron, frozen calculations in the same approximation.

We use the $p$-wave effective core potential and find that the calculated energy using this potential for the $5s$ orbital is 22.3 eV, which compares reasonably well with the 23.4-eV experimental value. This is the energy calculated on the finite-difference grid, as described below.

Thus we obtain the following equation for the time evolution of the valence orbitals:

$$i\frac{\partial}{\partial t}\varphi_i(\mathbf{r},t)=[-(\tfrac{1}{2})\nabla^2+V_{\rm ECP}(r)+V_{\rm Coul}(\mathbf{r})+V_{\rm XC}(\mathbf{r})+V_I(\mathbf{r})]\varphi_i(\mathbf{r},t)\ , \tag{4}$$

where $i=5s$ and $5p$ and

$$V_{\rm Coul}(\mathbf{r})=\int dr'\rho(\mathbf{r}')/|\mathbf{r}-\mathbf{r}'|\ . \tag{5}$$

In Eq. (5) the effective core potential is actually that generated as described above minus $V_{\rm Coul}+V_{\rm XC}$ evaluated using the total density of the initial electronic state. In a complete calculation, $V_{\rm Coul}$, and $V_{\rm XC}$ will be time-dependent functions of the electronic orbitals.

As described previously,[8] a finite-difference numerical technique is employed to integrate these coupled, partial differential equations. We use the fact that the Hamiltonian is symmetric around the $z$ axis and express the orbital functions in cylindrical coordinates, so that

$$\varphi_i(\mathbf{r},t)=\rho^{-1/2}\chi_i(\rho,z,t)e^{im\phi}\ . \tag{6}$$

Then we solve explicitly only for the two-dimensional wave functions $\chi_i$ by constructing a finite-difference grid in $\rho z$ space and approximating the kinetic energy terms using a three-point second derivative in each dimension. The time-dependent interactions maintain cylindrical symmetry, so that there is no mixing between different $m$ states. If circularly polarized light were used, this would no longer be true and the calculations would be significantly more complicated.

In these calculations, we solve the single-particle differential equation (4), with the potential terms frozen at their initial values. Only the matter-field interaction $V_I$ varies with time. We chose a laser pulse with a field which increases linearly over a preselected number of optical cycles, then which is held constant for several more periods so that an ionization rate for this orbital can be determined. This means the field amplitude $E(t)$ defined in Eq. (2) is given by $E(t)=E_0f(t)$, where

$$f(t)=\begin{cases}1/t_{\rm max}, & t<t_{\rm max}\\ 1, & t>t_{\rm max}\ .\end{cases} \tag{7}$$

If the chosen wavelength is far from resonance, we generally observe an exponential decay of the initial-state component in the time-dependent orbital during the constant intensity period, and identify this with the rate for multiphoton ionization.

Since the final state corresponds to a free electron, the wave function will grow in spatial extent with time. In order to keep the size of the calculation finite, we include an absorptive interaction on the outer edges of the grid. We add an imaginary part to the potential, which is nonzero only within approximately the last 10–20 grid points. The shape of the absorber is smooth enough to minimize any reflections. Its strength is large enough to reduce the flux which reaches the boundary to a negligible amount. Because of this absorption of the wave func-

tion, the time-dependent norm of the wave function decays, giving another measure of the ionization rate. As we will show in Sec. III, the rate of disappearance of the ground state and the rate of reduction of the total norm of the wave function are identical within the expected accuracy of the calculation for wavelengths far from resonance.

Numerical integration of the partial differential equation is accomplished using the Peacemann-Rachford propagator[13] and a time step corresponding to $\frac{1}{200}$ or $\frac{1}{400}$ of a laser period, depending on the wavelength. The spatial grid has a spacing in both dimensions of $0.3a_0$. We calculate the initial-state wave functions on the grid by propagating an initial guess in imaginary time until its energy becomes stable. The $5p_0$ and $5p_1$ orbital energies are found to be 12.32 and 12.23 eV, respectively, where $p_m$ is the $p$ orbital with $m_l=m$. Since these orbitals are not equivalent in the presence of a laser field polarized in the $z$ direction, we calculate ionization rates separately for each of them. In the fully coupled, many-electron calculations, these orbitals along with the $5s$ orbital will be included. The results from the frozen, single-electron calculations are presented in Sec. III.

## III. RESULTS

The multiphoton ionization of xenon has been studied experimentally by various groups using uv, visible, and ir wavelengths. The ionization process can be of very high order, and perturbation theory calculations become extremely demanding. Also, in these experiments, the intensities are high enough that nonperturbative effects become important. Using our direct integration of the time-dependent Schrödinger equation, we can allow for the most important high-intensity effects, the temporal shape of the pulse, and the nonperturbative strength of the electromagnetic field, which change the physics of the ionization dynamics.

In this section we present the results in terms of generalized cross sections or ionization rates according to the laser wavelength, with the shortest wavelength (lowest-order processes) coming first. After the results, we briefly discuss the breakdown of perturbation theory for increased laser intensities. This is followed by a description of resonance phenomena found for some wavelengths and for some ranges of intensity.

### A. Single-photon results

Single-photon ionization calculations were performed initially to test our model of the xenon atom. Because we choose the light to be polarized in the $z$ direction, the photoionization of the $5p_0$ orbital differs from that of the $5p_1$ (and $5p_{-1}$) orbitals. In the following we refer only to the $5p_1$ electrons but imply the inclusion of the equivalent $5p_{-1}$ electrons also. For the $5p_0$ initial state the $s$ and $d$ continua are both accessible, while for the $5p_1$ state only transitions to $d$ waves are allowed. We obtain the single-photon ionization cross sections by selecting an intensity weak enough that multiphoton processes are unimportant, then determine the decay rate of the initial state during the constant intensity period of the pulse. The intensity, however, must be large enough that significant ionization occurs in a reasonably short integration time so that the calculations remain finite. We check the linearity of the predicted rate with intensity by performing calculations at two intensities.

These cross sections compare well to exact results for this potential, which were generated using complex basis-set techniques.[14] We obtain, for example, a total cross section of 46 Mb at a photon energy of 14.4 eV compared with the exact value of 41 Mb and with the measured value of 60.1 Mb.[15] For a photon energy of 15.63 eV, the three values are 29, 27, and 54.5 Mb, respectively. Similar agreement was obtained for other photon energies; this is the sort of agreement with experiment one expects from a Hartree-Slater model. (See Kennedy and Manson.[16]) The calculated partial waves were also in good agreement with the exact results. We also consider the photoionization of the $5s$ orbital, calculating a cross section of $4.5\times10^{-20}$ cm$^2$ compared to an exact theoretical value of $5\times10^{-20}$ cm$^2$ for a photon energy of 24 eV. This cross section is the smallest we have ever calculated using this numerical technique.

### B. Two-photon results

We calculated the two-photon ionization rate at 193 nm as a further test of our model since there are several theoretical results for comparison, although these results are not for the same potential. We find the two-photon generalized cross section at this wavelength to be $4\times10^{-50}$ cm$^4$s compared to $1.5\times10^{-49}$ cm$^4$s calculated by l'Huillier and Wendin[17] in a Hartree-Fock picture and $2\times10^{-50}$ cm$^4$s by the same authors using random-phase-approximation with exchange. McGuire[18] obtained $8\times10^{-50}$ cm$^4$s using a Green's-function technique, and Gangopadhyay *et al.*[19] calculated $5\times10^{-51}$ cm$^4$s using a generalized multichannel quantum defect theory. Lambropoulos had also reported[1] a value of $1.6\times10^{-49}$ cm$^4$s. The latter three calculations were performed in $j$-$j$ coupling. Since this wavelength produces ionization only into the $^2P_{3/2}$ continuum, comparison with the other calculations, which all ignore spin-orbit interactions, may be misleading. However, above the $^2P_{1/2}$ threshold, where both continua are open, the results of Gangopadhyay *et al.* and McGuire show only a small increase in the total cross section, except at isolated resonance wavelengths. The experimental results at 193 nm also exhibit appreciable variation. The most recent, by McCown *et al.*[20] give a cross section of $4\times10^{-50}$ cm$^4$s in pretty good agreement with the calculated values. Two earlier measurements[21,22] were about two orders of magnitude smaller, both groups indicating their measurements were probably lower bounds.

### C. Three-photon results

We calculated three-photon ionization at two wavelengths and a range of intensities. The interest here is that for easily realizable intensities we find perturbation theory breaking down, with the ionization rate departing from an $I^3$ dependence above $5\times10^{13}$ W/cm$^2$. In Fig. 1, we show the calculated ionization rate for 293 nm be-

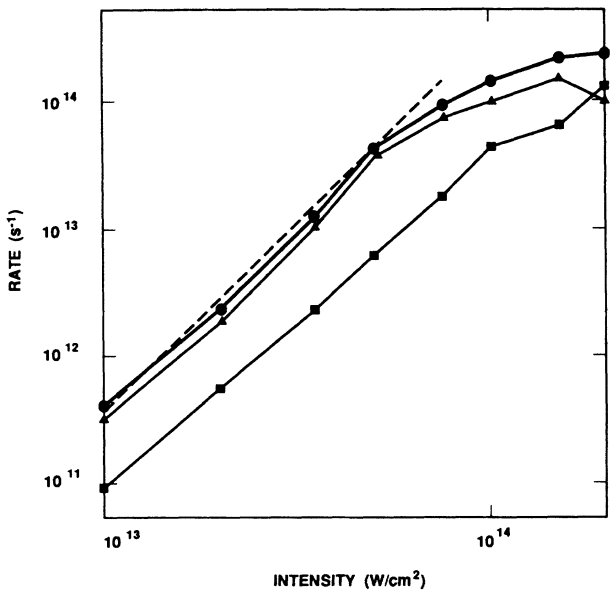


FIG. 1. Multiphoton ionization rates for xenon $5p_1$ (lowest curve) and $5p_0$ (next lowest) along with the total rate from the $p$ shell as a function of laser intensity for 293 nm. Dashed line is a fit to an $I^3$ dependence.

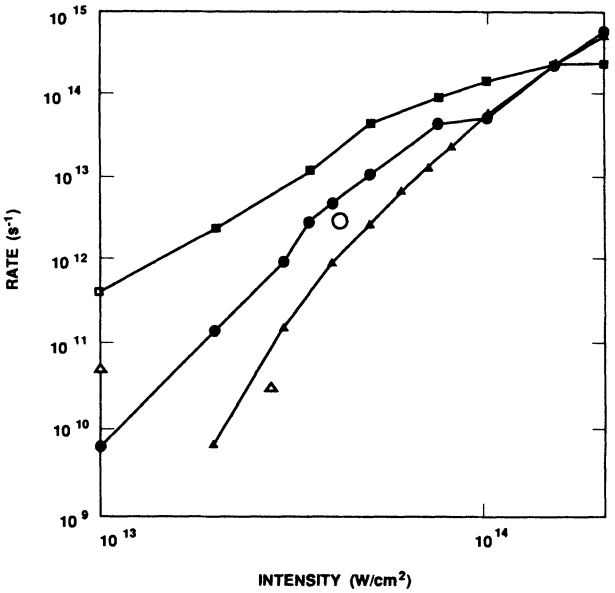


FIG. 2. Multiphoton ionization rates for the valence $p$ shell of xenon as functions of intensity for 293 nm (solid squares), 586 nm (solid circles), and 1064 nm (solid triangles). Open symbols denote experimental results.

tween $10^{13}$ and $2\times10^{14}$ W/cm$^2$. The symbols on the lines indicate the calculated points. The lower curve shows the predicted total rate for the four $5p_1$ and $5p_{-1}$ electrons. The next lower curve is for the $5p_0$ electrons, with the heavy solid line indicating the total rate for the $p$ shell. We also calculated the rate for the $5s$ electrons at this wavelength and found that it was orders of magnitude smaller. The rate at $10^{14}$ W/cm$^2$ was found to be less than $10^{11}$ s$^{-1}$. The dotted line in Fig. 2 represents a fitted $I^3$ rate, and illustrates the departure of the calculated results from the perturbative behavior at higher intensities. The generalized cross section corresponding to this line is $1\times10^{-82}$ cm$^6$s$^2$, which agrees to within about 20% with the Green's-function results of McGuire[18] but is over six orders of magnitude smaller than that reported by Gangopadyay *et al.*,[19] $3\times10^{-76}$ cm$^6$s$^2$. (An error in a conversion factor in their three-photon calculations, was discovered and they now obtain results which are in good agreement with our result.[23]) We know of one experimental result at this wavelength by Perry *et al.*[24,25] who measured an ionization rate of $4\times10^{11}$ s$^{-1}$ for a peak intensity of $1\times10^{13}$ W/cm$^2$. This corresponds to a three-photon cross section of $1.2\times10^{-82}$ cm$^6$s$^2$. At 266 nm, which produces electrons with energies above the second ionization threshold, we obtain a three-photon cross section of $2.5\times10^{-82}$ cm$^6$s$^2$ versus $5\times10^{-82}$ cm$^6$s$^2$ from McGuire and $5\times10^{-76}$ cm$^6$s$^2$ from Gangopadhyay *et al.*

### D. Six-and eleven-photon results

In considering the longer-wavelength regime commonly used in experiments, we have obtained results for the following two case: 1064 and 586 nm. These represent, in lowest-order perturbation theory, 11th- and 6th-order ionization, respectively. In Fig. 2 we show the calculated ionization rates for these two wavelengths along with those for 293 nm, discussed above, for laser intensities between $1\times10^{13}$ and $2\times10^{14}$ W/cm$^2$. Only in the case of the three-photon ionization, the shortest wavelength, is the rate proportional to a power of the intensity, at least for the lower part of this range. All rates are saturated by $1\times10^{14}$ W/cm$^2$, indicating the onset of the tunneling mechanism or the presence of resonances as discussed below.

Also shown by the open symbols in Fig. 2 are some experimental rates derived from reported saturation intensities which were determined in the following way. Saturation in the experiments occurs because at some intensity, all atoms in the focal volume of the laser are ionized before the pulse is over. Increasing the intensity cannot produce any more ions from this volume. This is different from the saturation discussed above where the departure from perturbation theory by the rate is considered "saturated" because the rate is found to be less than that which would be predicted from the extrapolation of the power law. Therefore we take the reported saturation intensity and assume that the corresponding rate is three times the inverse of the pulse length. This means that we would predict that the population of neutrals had been reduced by at least half, depending on the particular pulse shape, during the pulse. This is somewhat arbitrary, but good enough to show, in general, the consistency of the measured rates with our calculated results. There is the single measurement by Perry *et al.*[24,25] plotted as an open square at $1\times10^{13}$ W/cm$^2$ for 293 nm and a single point, denoted by an open circle, at $4.2\times10^{13}$ W/cm$^2$ for 586 nm by the same group.[26]

There are two recent results for 1064 nm, one at $1\times10^{13}$ W/cm$^2$ by l'Huillier *et al.*[27] and one from Freeman *et al.*[28] at $2.8\times10^{13}$ W/cm$^2$, which are denoted by the open triangles. We have obtained excellent agreement with all the measurements except the rate reported by l'Huillier *et al.* The uncertainty in their absolute intensities may be as large as a factor of 50%,[29] which would lead to better agreement with our calculations and the other experimental result.

### E. Breakdown of perturbation theory

The departure from perturbation theory, as illustrated by the rates shown in Fig. 1, can be attributed to a second mechanism for ionization becoming important at higher intensities. In very strong laser fields, the electrons can tunnel from the atom into the continuum rather than being excited by absorbing $n$ photons. In the work reported here, the ionization may not be in the real tunneling regime, but in the transition regime between the perturbation and tunneling regimes. Theoretical treatment of this phenomenon was first discussed by Keldysh[30] and later revised and extended by Reiss[31] and Faisal.[32] We also found that the ionization rate in general was slower from the $p$ orbitals perpendicular to the direction of polarization, with the difference being most pronounced at the longer wavelengths. What is interesting in the 293-nm results is that the departure from perturbation theory occurs first for the $5p_0$ orbitals, which are pointed in the direction of the laser polarization. The advent of the tunneling or diffusion mechanism above $5\times10^{13}$ W/cm$^2$ for the $5p_0$ electrons leads to a relative decrease in their ionization rate compared to the $5p_1$ rates which are still increasing as $I^3$. One might have expected an enhancement in the $5p_0$ ionization rate because the orbital, extending much more in the direction of the polarization, should be much more likely to escape by tunneling through the barrier, but exactly the opposite effect on the rate is found. At the highest intensities shown in Fig. 1 resonance effects have become important and the rates for the two different initial orbitals actually cross.

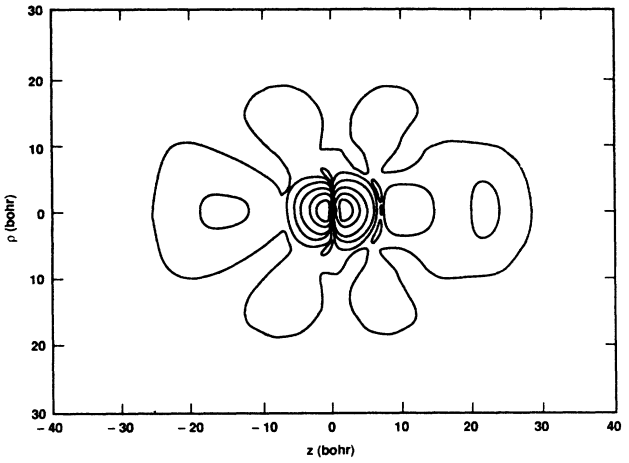


FIG. 3. Excited resonance state for the $5p_0$ initial state at $3.5\times10^{13}$ W/cm$^2$ and 586 nm.

### F. Resonance effects

As mentioned above, we also have found some evidence for the excitation of resonances in our calculations. In Fig. 2, we find that the rate for 586-nm photons shows an interesting jump just above $3\times10^{13}$ W/cm$^2$. By looking at the time-dependent wave function, we see that at $3.5\times10^{13}$ W/cm$^2$ a strong excitation of a temporarily bound, but highly excited state occurs. A contour plot of the excited-state wave function is reproduced in Fig. 3.

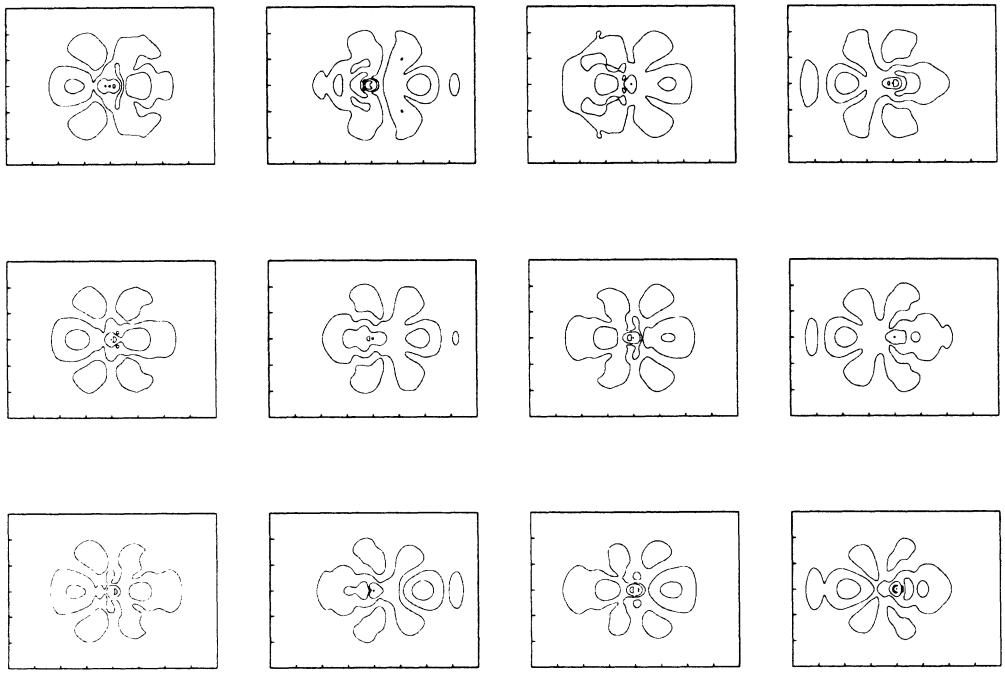

FIG. 4. Time-dependent behavior of the resonance wave function over three optical cycles.

We obtain this figure by stopping the ionization calculation at some point during the constant intensity period and plotting the total electron density of the time-dependent wave function. Each successive contour shows a density change of one order of magnitude. From the nodal structure of the wave function, we conclude that it is dominated by a large $l=3$ component. This must be due to either a four- or six-photon excitation of an $f$ orbital whose energy has been shifted into resonance by the dynamic Stark effect. We can investigate the behavior of this excited, resonance state by itself by orthogonalizing the time-dependent wave function to the initial state at this instant in time; then propagating the projected wave function, still subject to the constant field, for several optical cycles. In Fig. 4 we show snapshots of this projected wave function over three optical cycles. Note that the orbital density oscillates back and forth with the field, but does not change its general shape. Doing this we observe an exponential decay of the remaining wave function, due to further excitation into the continuum, with a rate constant of $9.7\times10^{13}$ $s^{-1}$. This is significantly faster than the rate of excitation of the resonance from the ground state, which is about $1.4\times10^{12}$ $s^{-1}$. If the initial state is chosen to be the $5p_1$ orbital, this resonance state is not observed. This is probably due to the different ac Stark shift of the comparable $f$ state with $m=1$. For comparison with the resonance state in Fig. 3 we plot the wave function after the same elapsed time for the intensity just below the resonance, $3\times10^{13}$ W/cm$^2$, in Fig. 5. This shows no comparable resonance structure, but does show the collimation of the outgoing flux along the direction of polarization. As a function of time, this wave function does vary noticeably, exhibiting no structure as seen in the resonance case. As the intensity is further increased, the resonance state disappears gradually, with the excited state at $1\times10^{14}$ W/cm$^2$ showing no obvious $l=3$ component. Therefore this bound state has been tuned through resonance by varying the field intensity.

The presence of a resonance state should result in narrow peaks in the electron energy distributions, as has

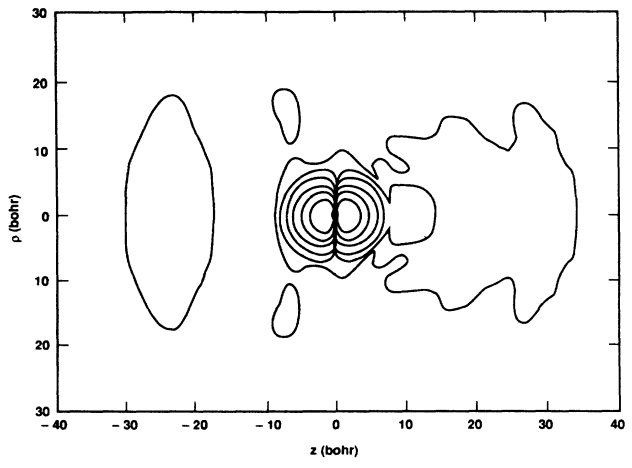


FIG. 5. Time-dependent ionizing wave function for the $5p_0$ initial state at $3\times10^{13}$ W/cm$^2$ and 586 nm.

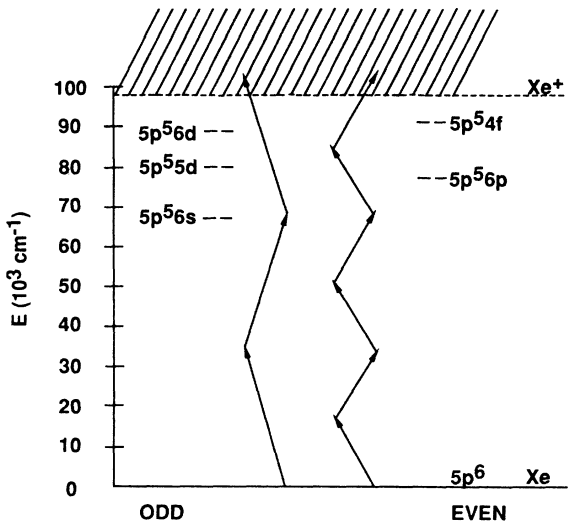


FIG. 6. Energy levels of xenon which may contribute to observed resonances.

been proposed and observed by Freeman, *et al.*[33] in their very short pulse (400 fs) multiphoton ionization (MPI) experiments at 616 nm. The width corresponding to our calculated ionization rate out of the resonant state is less than 0.1 eV, which is similar to that observed experimentally.

We have attempted to identify the state responsible for this structure by considering the field-free energy levels of xenon which are shown in Fig. 6. Arrows indicate multiphoton absorption paths. The ladder on the right corresponds to 293-nm photons and on the right to 586-nm photons. Arrows tilted to the right will populate even parity states and those to the left, the odd states. Using the calculated excitation energy of 11.45 eV for the $4f$ state determined on this finite-difference grid and adding an ac stark shift for this state of 1.13 eV, which we assume, as did Freeman *et al.*,[33] is equal to the total ponderomotive shift,

$$E_p=e^2F^2/4m\omega^2\ , \tag{8}$$

we see that this is very close to being resonant with $6\hbar\omega$ at 12.67 eV. This is one of the states that Freeman *et al.* speculated might be responsible for one of the series of peaks they saw in their electron distributions. The fact that our $4f$ excitation energy is somewhat higher than the true energy, 11.27 eV, means that we see this resonance with shorter wavelength, or lower intensity, than we would predict for the real atom. These calculations do not include exact excitation energies, but are qualitatively accurate in their predictions of these resonance effects. In fact, if this resonance did shift to slightly higher intensity, our calculated rate and the measured rate of Perry *et al.* would probably be in even better agreement.

At intensities above $1\times10^{14}$ W/cm$^2$ for 293-nm photons, we also find a resonant state playing an important role in the excitation process. In Fig. 7 we show the time-dependent wave function for $2\times10^{14}$ W/cm$^2$ for the $5p_0$ initial state which exhibits a very strong $d$-state reso-

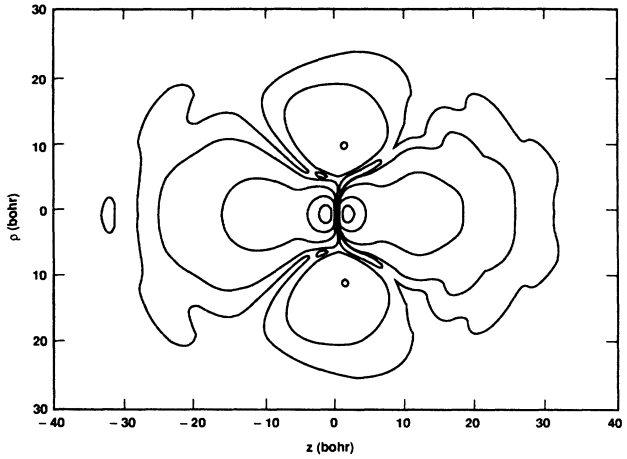


FIG. 7. Excited resonance state for the $5p_0$ initial state at $2\times10^{14}$ W/cm$^2$ and 293 nm.

nance. This resonance has a very different effect on the preionization dynamics compared to the previous case because it is found to decay more slowly into the continuum than back into the initial state. In Fig. 8 we show the time-dependent norm of the wave function for the calculation at $5\times10^{13}$ W/cm$^2$, where the field is increased over five optical cycles, then is constant for 15 cycles. The solid line is the norm and the dashed line is the absolute value squared of the overlap of the propagated wave function with the initial $5p_0$ orbital. The norm is found to decay at the same rate of overlap, indicating that the ionization takes place by excitation from the initial state directly into the continuum. In contrast, Fig. 9 shows the same information but for the case of $2\times10^{14}$ W/cm$^2$, but with the constant intensity interval extended to 25 cycles. In this case, Rabi oscillations between the ground

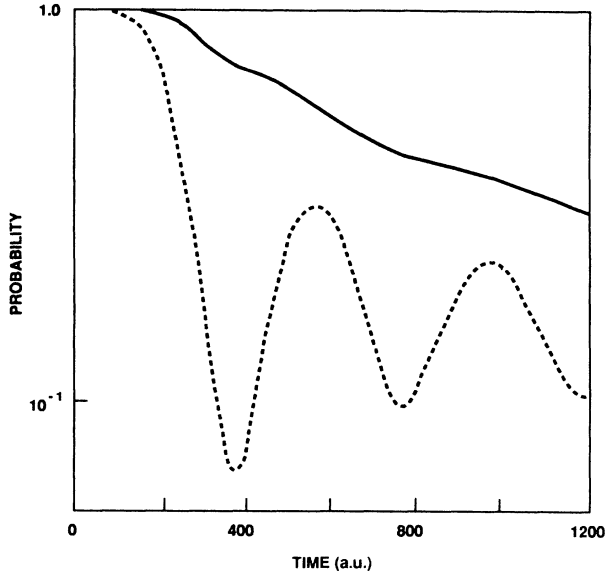


FIG. 9. Time-dependent norm of the wave function (solid line) and absolute square of the overlap with the initial $5p_0$ state (dashed line) for $2\times10^{14}$ W/cm$^2$ and 293 nm.

and resonance states are present. This is a semilog plot which shows that after a brief transient period, an approximately exponential decay is found, even though the Rabi oscillations are strongly pronounced. Changing the period for turning on the laser field by doubling it does not affect these results. As described above we can investigate the time evolution of the excited state alone by projecting out the ground-state component and propagating the excited state in the presence of the field. In Fig. 10, the semilog plot of the time-dependent norm of this pro-

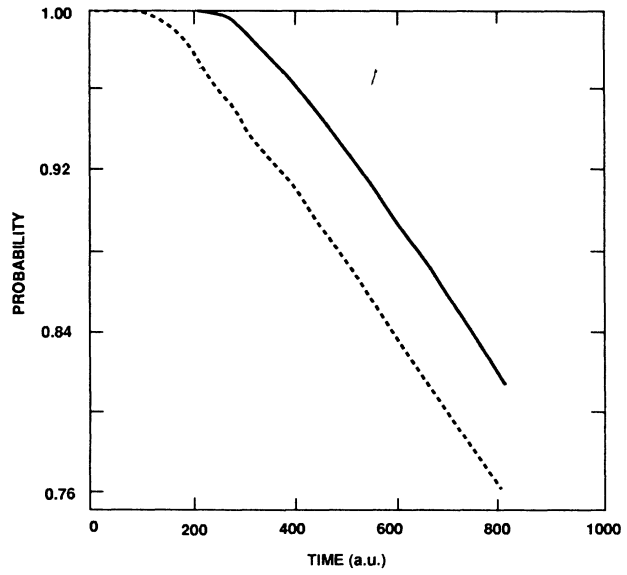


FIG. 8. Time-dependent norm of the wave function (solid line) and absolute square of the overlap with the initial $5p_0$ state (dashed line) for $5\times10^{13}$ W/cm$^2$ and 293 nm.

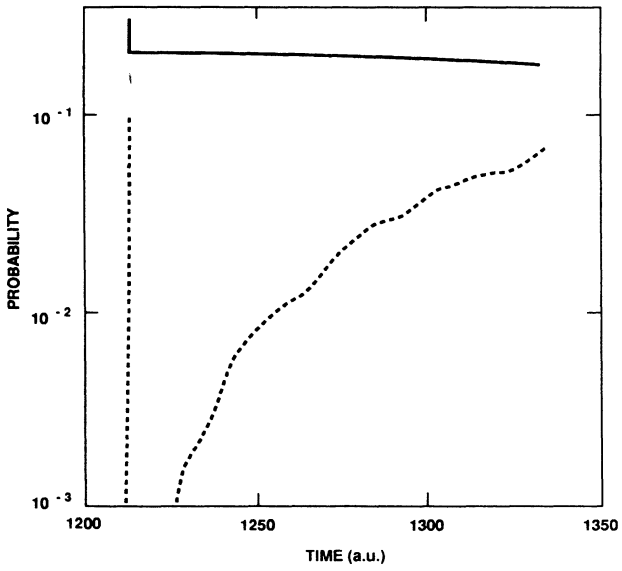


FIG. 10. Time-dependent norm of the projected $d$-wave resonance wave function (solid line) and absolute square of the overlap with the initial $5p_0$ state (dashed line) for $2\times10^{14}$ W/cm$^2$ and 293 nm.

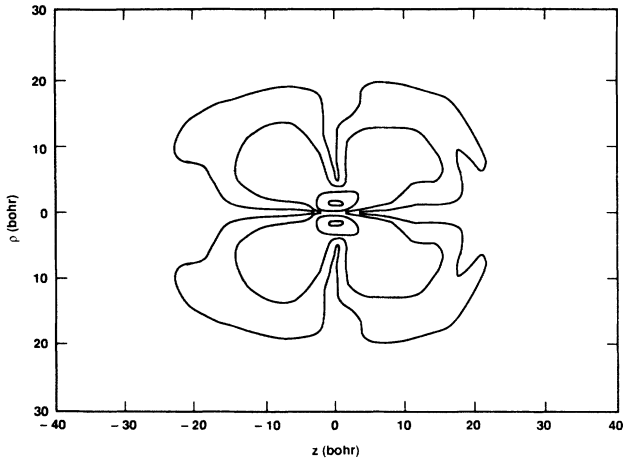


FIG. 11. Excited resonance state for the $5p_1$ initial state at $2\times10^{14}$ W/cm$^2$ and 293 nm.

jected wave function is seen to decay exponentially, with a rate of $5\times10^{13}$ s$^{-1}$, and the projection onto the initial state, shown by the dashed line, grows rapidly over three optical cycles of the field. The vertical sections of the curves indicate the reductions of these functions due to the orthogonalization to the initial state at $T=1211$ a.u. (1 a.u.$=2.42\times10^{-17}$ s). In this case, because the decay out of the resonance to the continuum is so slow, we found a reduction in the ionization rate as the intensity was increased from $1.5\times10^{14}$ to $2\times10^{14}$ W/cm$^2$. (See Fig. 1.) This resonance is also present in the $5p_1$ ionization for intensities above $1\times10^{14}$ W/cm$^2$. We show the resonance wave function for this initial state for the intensity of $2\times10^{14}$ W/cm$^2$ in Fig. 11. In this case it is an $m=1$ $d$ orbital which is excited. In both the $5p_0$ and $5p_1$ calculations, the resonance is noticeable in the time-dependent wave function for $1\times10^{14}$ W/cm$^2$ and above. It is not completely clear why the $5p_1$ and $5p_0$ rates cross, except that the transition moment into the continuum may be changing significantly with the intensity along with the Stark-shifted energy of the resonance. Also the $5p_1$ rates are for four electrons, compared to the $5p_0$ rate which is for two electrons. If we had plotted the rate per electron, these curves would not have crossed.

The calculated decay rate of the $m=1$ $d$-wave resonance is found to be $4\times10^{13}$ s$^{-1}$ at $2\times10^{14}$W/cm$^2$, in good agreement with the $m=0$ state. The $5p_0$ and $5p_1$ orbitals in our calculation are not exactly equivalent due to the differences in the distributions of grid points in these two dimensions, so that some difference in the two rates as functions of intensity could be caused by these slight differences also.

We can attempt to identify the principle quantum number of these $d$-state resonances in the same way we determined the existence of the $4f$ state for 586 nm. The excitation of a $d$ state can only occur through the absorption of three photons; no single-photon excitation is probable due to the huge energy gap from the ground state to the first $d$ state. The second $d$ state, which is experimentally known to lie at about 11 eV as shown in Fig. 6, is a prime candidate, provided we can assume that the Stark shift is comparable to the ponderomotive shift. In this case $E_p$ is equal to about 1.6 eV at $2\times10^{14}$ W/cm$^2$, which again would move this state to the vicinity of three photons at 12.69 eV. Also it is possible that some higher Rydberg $d$ state is responsible, but it is difficult to determine accurate excitation energies for these highly excited states on the grid. Again the decay rates of these resonances are small enough that very narrow peaks, on the order of a few hundredths of an electron volt, in the electron energy distributions should be observed.

The plotted ionization rates for 293 nm in this intensity regime are approximate because the decay is not purely exponential, as can be seen in Fig. 7. The theoretical error bars on these rates are the largest of all those rates presented (probably no more than a factor of 2), except perhaps for those in Fig. 2 below $10^{10}$ s$^{-1}$ where the accuracy of the calculation suffers from numerical instabilities. As was pointed out before,[8] when the ionization rate drops below this value, the change in the wave function per integration time step drops into the numerical noise of the integration. With a time step on the order of $10^{-17}$ s, a change in the wave function of less than one part in $10^7$ for the calculated properties is very difficult to detect.

The results at 1064 nm showed no resonance effects, with the final state exhibiting a strongly collimated flux along the direction of polarization and with a portion of the wave function being emitted first in one direction during the first half of the optical cycle, then in the opposite direction in the second half. Figure 12 shows a snapshot of the excited-state wave function, illustrating this behavior from a calculation at $1\times10^{14}$ W/cm$^2$. This phenomenon was first seen in our helium calculations and is good evidence that the tunneling mechanism is in effect.

## IV. CONCLUSIONS

We have reported the calculation of the multiphoton ionization of the outer valence shell of xenon by a linearly polarized laser in the single-particle, frozen approximation. The results for 1- to 11-photon ionization are found to be in quite good agreement with most of the existing

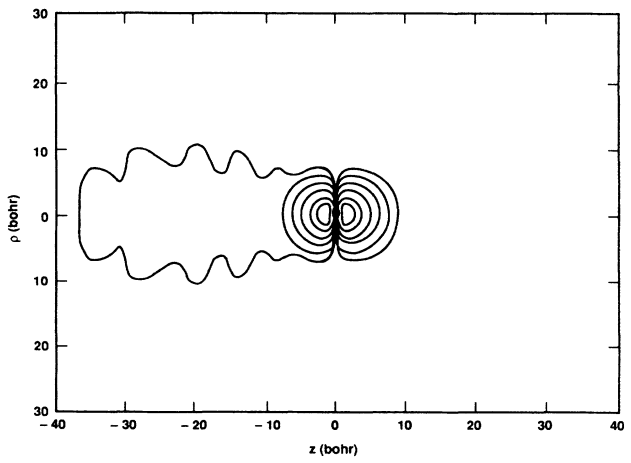


FIG. 12. Time-dependent ionizing wave function for the $5p_0$ initial state at $1\times10^{14}$ W/cm$^2$ and 1064 nm.

measured rates. Our calculations agree well with the results of Perry *et al.*[24–26] at 293 and 586 nm, with Freeman *et al.*[28] for 1064 nm, but may be inconsistent with those of l'Huillier *et al.*[27] at 1064 nm. Excellent agreement for the lower-order processes with other theoretical results were obtained also.

These calculations require 200–400 s on a Cray XMP computer to determine an ionization rate for a given wavelength and intensity. If resonance behavior is encountered, longer integration times may be required to give a complete picture of the preionization dynamics. The method does not lend itself well to the determination of the final-state electron energy distributions because of the finite size of the grid. It is not practical in a two-dimensional numerical calculation to follow the ionized wave function into the asymptotic region to determine its energy components, due to the long integration times required. Excellent results for these distributions exist for several one-dimensional and Keldysh models[5,24,25,26,31,34,35] and recently[36] have been obtained for a three-dimensional calculation for hydrogen using an expansion of the wave function in spherical harmonics and a numerical representation of the radial degree of freedom. Therefore our emphasis on total ionization rates and on the details of the preionization dynamics complements the excellent analyses available for the final-state energy distribution.

We can, however, say something about the angular distributions of the ejected electrons. In general, for long-wavelength multiphoton processes, we find the outgoing flux collimated along the direction of polarization consistent with the electron distributions measured. We predict, for the ionization out of the resonant states we discovered, that the angular distribution should be dominated by the absorption of one more photon, producing a $g$-wave (with some $d$-wave) distribution from the $4f$ resonance state at 586 nm, with an energy consistent with having absorbed seven photons. From the $6d$ resonances at 293 nm, the final angular momentum distribution should be predominantly $f$ wave with some admixture of $p$ wave at an energy corresponding to four-photon absorption. Thus a signature of these resonance states will be a significant change as a function of intensity in the angular distributions of the electrons emitted at the appropriate energies. The determination of the precise energy at which they will be measured depends on the shape of the pulse used because of ponderomotive effects.

One important result from these calculations worth emphasizing is that the ionization out of the $p$ orbital aligned along the direction of polarization was much more rapid than for the other orbitals for all wavelengths studied. At 1064 nm, the difference in rates per electron was more than a factor of 20. This means that the residual ion is predicted to be left in an oriented final state. It also indicates that one should be cautious about relying on Keldysh- or Reiss-model calculations for total ionization rates in which the initial state is usually assumed to be a screened $s$ orbital rather than a particular $p$ orbital, although they have been remarkably successful.

The effects of relaxing the orbitals of the other valence electrons will be the subject of future work, using the model described above. We believe that most of the interesting effects of the other electrons will be seen only at the higher range of intensities studied here. One must beat the single-ionization processes, either by using much shorter pulses or by finding resonances such as the $6d$ state at 293 nm in which the excitation is trapped in the atom for some useful amount of time. The multielectron calculations will be able to show whether this resonance excitation energy is shared with the other outer electrons or if several electrons are excited simultaneously before ionization occurs. It also seems to be true that shorter wavelengths are more likely to be effective in exciting these states. The longer-wavelength results do not show any propensity to exhibit resonances at high intensities. The broadening of resonances at high intensities is clearly much more efficient for longer wavelengths. Since the ionization rates were all found to be in excess of $10^{13}$ s$^{-1}$ for intensities above $1\times10^{14}$ W/cm$^2$, pulses of a few tens of femtoseconds may be needed to explore this regime. For such pulses, our calculations can easily be performed for real pulse shapes since the integration time will be so short. Some of the calculations reported here corresponded to integration times of more than 0.1 ps.

Finally, we note that in our TDHF helium calculations[8,37] we also found resonance structures at very high intensities $>5\times10^{14}$ W/cm$^2$. These did not show the obvious structure of a single partial wave, but appeared as some portion of the excited wave function trapped in the vicinity of the atom, oscillating back and forth with the field and decaying with a rate which was different from the excitation rate from the initial state. They appeared to be trapped by the ponderomotive barrier and many partial waves may have been contributing. It seems likely that these resonance effects play very significant roles in the preionization dynamics at high intensities in most systems.

These calculations show that we now have a reliable tool for studying multiphoton ionization for wavelengths and intensities currently being used in the laboratory. Ionization rates and the effects of Stark-shifted intermediate resonant states show good agreement with the existing experimental data. However, since our effective potential is approximate, we must allow for the excited-state energies being slightly shifted from the true values. In the near future, laser intensities are projected to exceed those considered here by many orders of magnitude. One problem in studying such high intensities with numerical methods is that the oscillatory motion of the free electrons due the the laser field will have an extent far greater than the size of the atom. At $1\times10^{17}$ W/cm$^2$ and 248 nm, a free electron will oscillate over a distance of $100a_0$. Therefore, calculations of ionization using this method must allow for this jitter motion in order to determine whether the electron has actually left the atom. Progress on this problem is needed before the experiments from the next generation of lasers can be studied.

## ACKNOWLEDGMENTS

The author would like to thank Tom Rescigno for determining the effective core potential used in these cal-

culations. Also, he wishes to acknowledge many stimulating discussions about this work with Charles Cerjan, Bruce Shore, Mike Perry, Phil Bucksbaum, and Abraham Szöke. The work has been performed under the auspices of the U. S. Department of Energy by the Lawrence Livermore National Laboratory under Contract No. W-7405-ENG-48.

[1]P. Lambropoulos, Phys. Rev. Lett. **55**, 2141 (1985).
[2]S. Geltman, J. Phys. B **10**, 831 (1977).
[3]K. C. Kulander, Phys. Rev. A **35**, 445 (1987).
[4]C. Cerjan and R. Kosloff, J. Phys. B **20**, 4441 (1987).
[5]J. M. Javanainen and J. H. Eberly, J. Phys. B **21**, L93 (1988).
[6]M. S. Pindzola and C. Bottcher, J. Opt. Soc. Am. B **4**, 752 (1987).
[7]A. Kerman and S. E. Koonin, Ann. Phys. **100**, 332 (1976).
[8]K. C. Kulander, Phys. Rev. A **36**, 2726 (1987).
[9]Many excellent reviews and collections of articles exist. See, for example, J. Opt. Soc. Am. B **4**, 705 (1987).
[10]F. Herman and S. Skillman, *Atomic Structure Calculations* (Prentice Hall, Englewood Cliffs, NJ 1963).
[11]L. Kahn, P. Baybutt, and D. G. Truhlar, J. Chem. Phys. **65**, 3826 (1976).
[12]P. A. Christiansen, Y. S. Lee, and K. S. Pitzer, J. Chem. Phys. **71**, 4445 (1979).
[13]R. S. Varga, *Matrix Iterative Analysis* (Prentice Hall, Englewood Cliffs, NJ 1962).
[14]A. E. Orel and T. N. Rescigno, Chem. Phys. Lett. (to be published).
[15]G. V. Marr and J. B. West, At. Data Nucl. Data Tables **18**, 497 (1976).
[16]D. J. Kennedy and S. T. Manson, Phys. Rev. A **5**, 227 (1972).
[17]A. l'Huillier and G. Wendin, Phys. Rev. A **36**, 4747 (1987).
[18]E. J. McGuire, Phys. Rev. A **24**, 835 (1981).
[19]P. Gangopadhyay, X. Tang, P. Lambropoulos, and R. Shakeshaft, Phys. Rev. A **34**, 2998 (1986).
[20]A. W. McCown, M. N. Ediger, and J. G. Eden, Phys. Rev. A **26**, 3318 (1987).
[21]W. K. Bischel, J. Bokor, D. J. Kligler, and C. K. Rhodes, IEEE J. Quantum Electron **QE-15**, 380 (1979).
[22]R. V. Hodges, L. C. Lee, and J. T. Mosley, Int. J. Mass Spectrom. Ion Phys. **39**, 133 (1981).
[23]P. Lambropoulos (private communication).
[24]M. D. Perry, O. L. Landen, and E. M. Campbell (unpublished).
[25]M. D. Perry, Ph. D. thesis, University of California, Berkeley, 1988 (unpublished).
[26]M. D. Perry, O. L. Landen, A. Szoeke, and E. M. Campbell, Phys. Rev. A **37**, 747 (1988).
[27]A. l'Huillier, L. A. Lompre, G. Mainfray, and C. Manus, Phys. Rev. A **27**, 2503 (1983).
[28]R. R. Freeman, P. H. Bucksbaum, H. Milchberg, S. Darak, D. Schumacher, and M. E. Geusic, Phys. Rev. Lett. **59**, 1092 (1987).
[29]A. l'Huillier (private communication).
[30]L. V. Keldysh, Zh, Eksp. Teor. Fiz. **47**, 1945 (1964) [Sov. Phys.—JETP **20**, 1307 (1965)].
[31]H. R. Reiss, Phys. Rev. A **22**, 1786 (1980).
[32]F. H. M. Faisal, J. Phys. B **6**, L89 (1973).
[33]R. R. Freeman, T. J. McIlrath, P. H. Bucksbaum, and M. Bashkansky, Phys. Rev. Lett. **57**, 3156 (1986).
[34]P. H. Bucksbaum and M. Bashkansky, Phys. Rev. A (to be published).
[35]L. A. Collins and A. L. Merts, Phys. Rev. A **37**, 2415 (1988).
[36]M. R. Hermann and J. A. Fleck, Jr. (unpublished).
[37]K. C. Kulander, in *Proceedings of the IVth International Conference on Multiphoton Processes,* edited by S. J. Smith and P. L. Knight (Cambridge University Press, Cambridge, 1987).